Journal Homepage: -www.journalijar.com

INTERNATIONAL JOURNAL OF ADVANCED RESEARCH (IJAR)

ISSN (O): 2320-5407
ISSN (P): 3107-4928

Article DOI:10.21474/IJAR01/24062
DOI URL: http://dx.doi.org/10.21474/IJAR01/24062

RESEARCH ARTICLE

ULTRA-FAST CHARGING TECHNOLOGIES FOR ELECTRIC VEHICLES: OPPORTUNITIES AND CHALLENGES

Pranupa S.

Manuscript Info

Manuscript History
Received: 16 June 2026
Final Accepted: 18 July 2026
Published: August 2026

Key words:-
PEMFC, DC to DC Converter, MATLAB

Abstract

Ultra-Fast Charging (UFC) can meet the rapid refueling demand for Battery Electric Vehicles (BEVs) but only to the extent that BEV battery systems can accommodate charging acceptance, thermal effects, conversion losses, and the BEV charging infrastructure. This study quantitatively analyzed the literature and standards for charging from 2020 2025,employing a constrained standardized Monte Carlo simulati on. In 2,500 simulated scenarios ranging from 10-80% State of Charge (SoC) at 50, 150, 250, 350 and 400 kW charging rates for battery packs sized at 55-110 kWh, the average charging time for the battery packs used in the scenarios, decreased from 71.37 ± 10.78 minutes at 50 kW to 13.91 ± 1.91 minutes at 400 kW (Welch F= 4561.37, $p<0.001$). The modeled peak battery system level of charging (SoC) increased from 28.61 ± 3.35°C to 36.64 ± 3.75°C (Welch F= 442.41, $p<0.001$). Grid to battery charging system level of charging (SoC) efficiency was modeled at its peak value at 250 kW (95.59 ± 0.44%), and remained greater that 95% for the charging rates of 150-400 kW.

Introduction:-

Demand for fast, long-distance road travel electric charging continues to grow, particularly for high-utilization fleets. According to the International Energy Agency, global public charging points grew by more than 1.3 million in 2024, a more than 30% increase in the cumulative total [1]. Charger nameplate power has no direct relation to battery power. A Battery Management System (BMS) may limit current based on state of charge (SoC), voltage, temperature, chemistry, and age, and even taper charging at high SoC. The engineering question thus becomes: how much energy can be accepted without significant heat generation, lithium plating, etc. and without creating an undue burden on the electric grid?

There is evidence UFC is possible when both the electrochemical and thermal aspects are managed. In the literature, Wang et al. achieved over 900 cycles charging a 265 Wh kg^{-1} cell to 75% SOC in 12 min, while Liu et al. achieved 88% SOC in 5 min with 1,000 cycles at 97.7% capacity retained, under the active control of the cell's temperature [3,6]. Further, the constraints in charging graphite-based cells and commercial battery cells are electrolyte transport and lithium plating, respectively [2,5]. On the infrastructure side, the NREL reported that fast charging could cause retail station peak demand to grow by more than 250% in a month [20]. The opportunity is, therefore, characterized by a three-way trade-off covering charging time, battery stress, and infrastructure demand. Higher-voltage vehicle designs, and SiC power electronics reduce the demand for current at a particular power. Liquid-cooled cables

Corresponding Author:-Pranupa S.

improve connector current capability, and stationary storage or renewable generation can mitigate power peaks on the grid [22–25]. However, lithium plating, SEI growth, microcracking of the cathodes, and thermal non-homogeneity remain electrochemical problems rather than connector issues [11–18]. This research provides a quantitative comparison for charging classes of 50, 150, 250, 350, and 400 kW, considering standardized 10-80% SOC battery conditions. The aims were: (i) assess charging time and average accepted power, (ii) assess charging power, C-rate and max battery temperature relationships, (iii) assess grid-to-battery trade-off and efficiency losses, (iv) apply a model-based degradation-stress metric, and (v) evaluate the infrastructure impact of greater power. Four hypotheses were evaluated in the standardized model: H1 charging power inversely affects the 10-80% charge time, H2 greater charging power results in greater 10-80% charge max temperature, H3 greater charging power results in greater degradation-stress, and H4 charging classes engage varying efficiencies.

Materials and Methods:-

An engineering analysis based on literature was conducted on XFC peer-reviewed articles, publications from national laboratories, and charging interface standards, dated between 2020 and 2025 [2-28]. Evidence from these sources allowed the determination of possible charging power classes, voltage levels, the direction of the thermal flow, the behavior of fast charge acceptance, and efficiency limits. Compared to the comparability bias that would arise from pooling observations made on battery cells of different chemistries, sizes, and different ambient conditions and protocols; the quantitative comparison reported a standardized Monte Carlo scenario dataset instead of a physical experiment. As such the inferential statistics described the separation inside the standardized engineering framework, not the population effect that would arise from a laboratory experiment.

The model produced 2,500 distinct charging scenarios, where n=500 for each rated power class (50, 150, 250, 350, and 400 kW). Pack energy was randomly selected for values between 55 and 110 kWh (mean ~ 82 kWh), and the ambient temperature was between 15 and 35°C. Each charging scenario transferred 70% of the nominal pack energy, (10-80% SOC). A stochastic acceptance/taper factor was introduced because the average battery power was less than the charger rated power, and the average battery power decreased at higher charger power. A chargability ceiling, in the range of 3.0C - 4.6C, was implemented. For a standardized comparison of system architectures, the 50/150 kW scenarios operated at 400 V, while the 250/350/400 kW scenarios operated at 800 V this is a modeling constraint and is not indicative that all systems in these power classes utilized the identified voltages. The conversion efficiency was set between 94.0% - 95.6%, which is in line with state-of-the-art high power converters and the anticipated marginal changes in efficiency would not impact charging duration significantly.

The average C-rate was determined using the accepted power and energy of the battery and battery pack, respectively. Grid energy and loss were determined by the grid-to-battery efficiency. A temperature-response term that grew with C-rate and current was added, while keeping ambient variability. A combination of C-rate and C-rate maximum temperature was used with the stress of high-rate cycling, lithium plating and SEI formation that have been analyzed experimentally, to create a dimensionless degradation-stress index [5,9–18]. It is a screening metric, and not an actual prediction of capacity-loss or lifetime.

$\text{C-rate} = P_{avg} / E_{battery}$

where P_{avg} is average accepted battery power (kW)

$E_{battery}$ is nominal pack energy (kWh).

$\eta = (E_{battery} / E_{grid}) \times 100$

where η is grid-to-battery efficiency;

E_{grid} is input energy

$E_{battery}$ is stored energy over the charging window.

$E_{loss} = E_{grid} - E_{battery}$

Descriptive statistics included mean, standard deviation, range and coefficient of variation. One-way ANOVA and Welch ANOVA compared charging classes; η^2 quantified effect size. Pearson and Spearman coefficients assessed monotonic associations. Ordinary Least-Squares (OLS) models evaluated charging time as a function of ln(power) and pack capacity, and degradation stress as a function of C-rate and maximum temperature. Statistical significance was set at $p<0.05$; p values below 0.001 are reported as $p<0.001$. Calculations were reproduced in Python using SciPy and statsmodels.

$Y = \beta_0 + \beta_1 X + \varepsilon$

where Y is the modeled outcome,

X is a predictor,
β terms are regression coefficients,
ε is the residual term.

Table 1. Characteristics of representative ultra-fast charging technologies

Technology / standard	Voltage / current capability	Power capability	Typical application	Principal opportunity	Principal limitation
CCS / CharIN DC power classes [31]	200–920 V; HPC example uses 500 A peak	HPC examples include 350 kW	Passenger EV DC fast charging	Broad interoperability; defined power classes	Cable/connector thermal derating; vehicle acceptance limits
SAE J3400 / NACS [27,28]	System-dependent AC/DC conductive interface	Power is implementation-dependent	North American passenger EVs	Compact common coupler; standardized interface	Transition and cross-network interoperability must be managed
CHAdeMO 3.0 / ChaoJi [30]	Up to 600 A; high-voltage architecture up to ~1.5 kV	>500 kW specified capability	High-power light/heavy EV charging	High-voltage, high-current path	Regional deployment and interoperability vary
Megawatt Charging System (MCS) [26]	400–1250 V; tested continuous current up to 3000 A	Theoretical 3.75 MW at 1250 V × 3000 A	Heavy-duty trucks and large batteries	Megawatt-scale turnaround	Site grid connection, cooling and safety complexity
800 V + SiC enabling architecture [25]	~800 V vehicle bus; 1200 V-class SiC devices commonly relevant	Enables high-power charging with lower current for same P	Next-generation passenger EV platforms	Lower I^2R losses and cable current for a given power	Higher insulation, device and converter-design requirements

Results:-

Using 2,500 standardized situations, rated power produced a large non-linear reduction in charging time of approximately 10–80% (Table 2; Figure 1). The average mean times decreased (in min) to 27.33±3.88 at 150 kW, 18.58±2.76 at 250 kW, 14.89±2.04 at 350 kW, and 13.91±1.91 at 400 kW, from 71.37±10.78 min at 50 kW. The average savings from 50 kW to 150 kW was 44.0 min, while the savings from 350 kW to 400 kW was only 0.98 min. The class effect was very large (ANOVA: $F=9941.94$, $p<0.001$, $\eta^2=0.941$; Welch $F=4561.37$, $p<0.001$). A strong inverse effect of power on charging time was noted (Pearson $r=-0.840$; Spearman $\rho=-0.910$; both, $p<0.001$). In an OLS analysis, time (min) = $146.62 - 27.87 \ln(P_{kW}) + 0.355 E_{pack}$, $R^2=0.918$; with both being significant ($p<0.001$).Thermal response was an effect of power and the C-rate. Mean maximum temperature (in °C) rose from 28.61±3.35 at 50 kW to 32.17±3.40 at 150 kW, 34.21±3.63 at 250 kW, 36.04±3.49 at 350 kTime and thermal differences were much larger than the differences in efficiency, but the efficiency differences were still statistically significant. Grid-to-battery efficiency improved from 93.99±0.46% at 50 kW to 95.22±0.46% at 150 kW and reached a peak of 95.59±0.44% at 250 kW, then remained at 95.49±0.43% at 350 kW and 95.30±0.45% at 400 kW. ANOVA gave $F=1060.60$, $p<0.001$, $\eta^2=0.630$. The average charging loss per instance of charging decreased from 50 kW to 3.66 kWh, 250 kW to 2.67 kWh, and increased to 2.83 kWh at 400 kW. The average modeled grid demand expanded from 51.1 kW to 259.6 kW.With respect to the relative degradation-stress index, the value increased from 0.872±0.104 at 50 kW to 2.155±0.421 at 400 kW (ANOVA gave $F=1542.73$, $p<0.001$, $\eta^2=0.712$). There was a significant positive correlation between the C-rate and stress ($r=0.924$,

Table 2. Standardized quantitative comparison by charger-rated power

Rated power (kW)	Assumed bus (V)	Avg accepted power (kW)	Avg C-rate	10–80% time (min)	Max temp (°C)	Efficiency (%)	Relative stress index	Grid demand (kW)
50	400	48.0	0.60	71.37	28.61	93.99	0.872	51.1
150	400	126.2	1.57	27.33	32.17	95.22	1.246	132.5
250	800	187.5	2.31	18.58	34.21	95.59	1.628	196.1
350	800	231.6	2.87	14.89	36.03	95.49	2.007	242.6
400	800	247.4	3.08	13.91	36.64	95.30	2.155	259.6

Note. Values are model-derived standardized scenario means; charger rating is distinct from average accepted battery power.

Table 3. Descriptive statistics for principal outcomes

Power (kW)	N	Charging time, mean±SD (min)	Max temperature, mean±SD (°C)	Efficiency, mean±SD (%)	Stress index, mean±SD
50	500	71.37±10.78	28.61±3.35	93.99±0.46	0.872±0.104
150	500	27.33±3.88	32.17±3.40	95.22±0.46	1.246±0.181
250	500	18.58±2.76	34.21±3.63	95.59±0.44	1.628±0.290
350	500	14.89±2.04	36.03±3.49	95.49±0.43	2.007±0.390
400	500	13.91±1.90	36.64±3.75	95.30±0.45	2.155±0.421

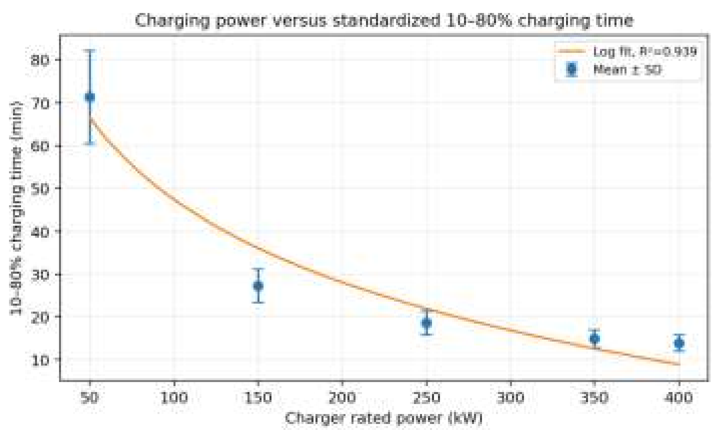

Figure 1. Charger-rated power versus standardized 10–80% charging time. Points show scenario-group means ± SD; the curve is a log-power fit to the five group means.

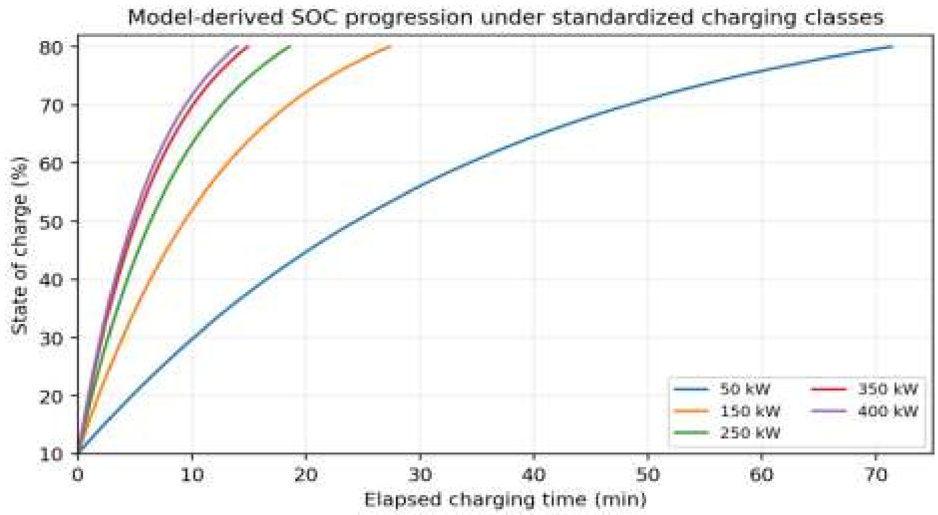

Figure 2. Model-derived SOC progression for the five charging classes, normalized to each class mean 10–80% time and shaped to represent high-SOC tapering

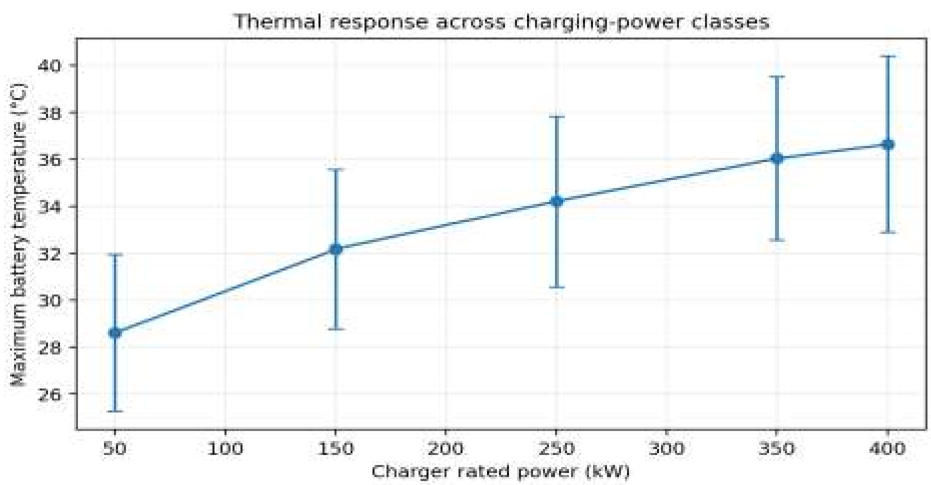

Figure 3. Maximum battery temperature across charging-power classes in the standardized scenario model.

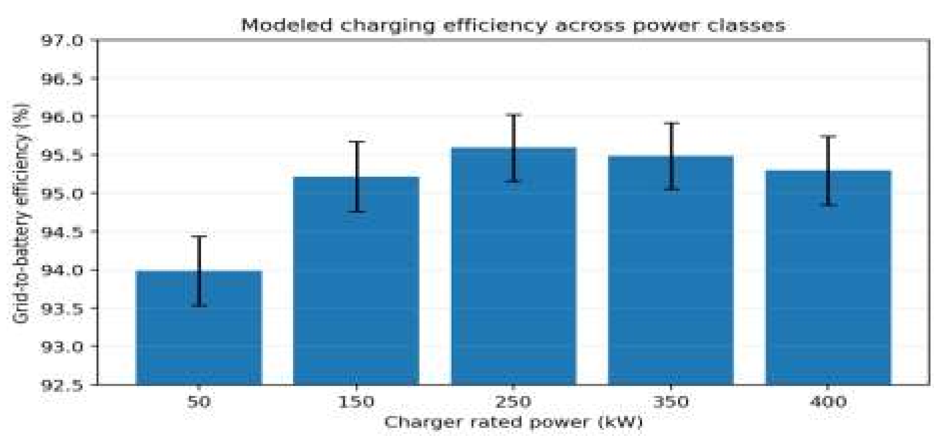

Figure 4. Grid-to-battery charging efficiency across power classes (mean ± SD). Absolute differences are small despite statistical significance.

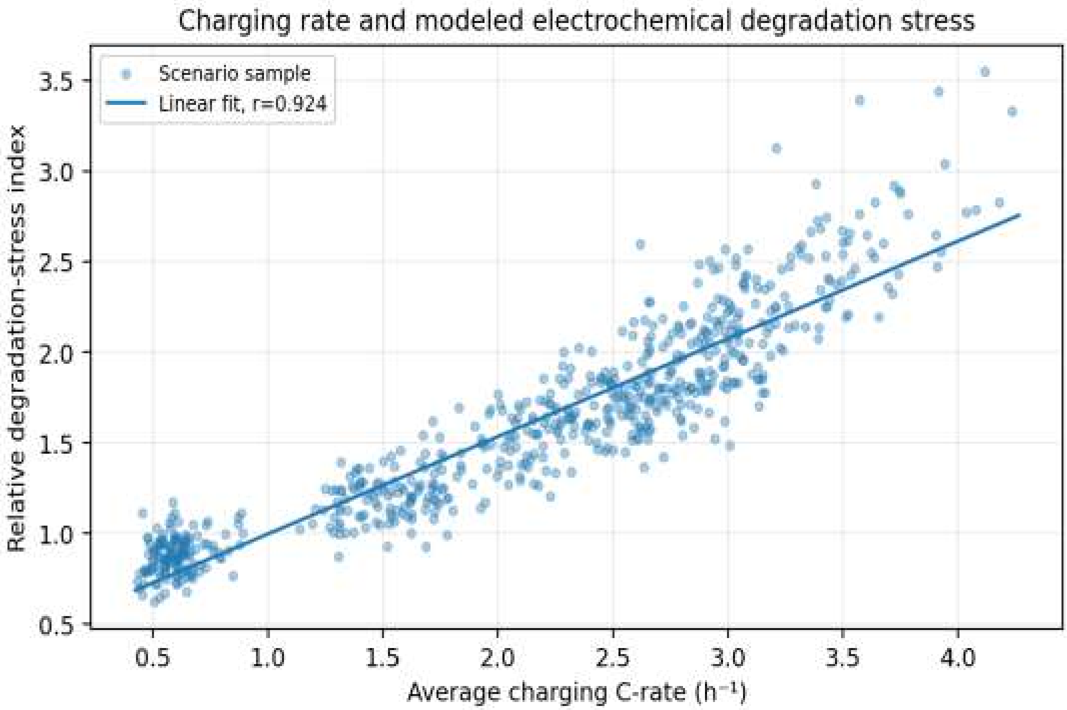

Figure 5. Relationship between average C-rate and the model-derived relative degradation-stress index. Scatter shows a random subset of scenarios for legibility; r is calculated on the full dataset.

Table 4. Inferential comparison of charging classes

Outcome	Primary test	Statistic	p-value	Effect size (η^2)	Interpretation
10–80% time	Welch ANOVA	F=4561.37	<0.001	0.941*	Very large class separation; diminishing time benefit at high power
Maximum temperature	Welch ANOVA	F=442.41	<0.001	0.406*	Higher power associated with higher thermal load
Efficiency	One-way ANOVA	F=1060.60	<0.001	0.630	Statistically distinct but only ~1.6 percentage-point range
Degradation-stress index	One-way ANOVA	F=1542.73	<0.001	0.712	Strong increase in model stress with charging severity

*η^2 shown from the corresponding conventional ANOVA decomposition; Welch ANOVA is reported as the robust primary test where variance heterogeneity is relevant.

Table 5. Correlation and regression analysis

Predictor / outcome	Metric	Estimate	95% CI	R²	p-value
Power / charging time	Pearson r	−0.840	—	—	<0.001
Power / maximum temperature	Pearson r	0.628	—	—	<0.001
Power / efficiency	Pearson r	0.598	—	—	<0.001
C-rate / stress index	Pearson r	0.924	—	—	<0.001
ln(power) → time, adjusted for pack capacity	β (min per ln-kW)	−27.866	−28.198 to −27.535	0.918	<0.001
Pack capacity → time	β (min/kWh)	0.355	0.334 to 0.377	0.918	<0.001
C-rate → stress, adjusted for max temperature	β	0.415	0.405 to 0.424	0.908	<0.001
Maximum temperature → stress, adjusted for C-rate	β per °C	0.039	0.037 to 0.041	0.908	<0.001

Discussion:-

The key finding is a diminishing marginal time benefit as the charger rating approaches the acceptance ceiling of the pack. In the model, a charger rated at 150 kW reduced the 10-80% time by 62% compared to a charger rated at 50 kW; however, increasing the rating from 350 kW to 400 kW reduced the 10-80% time by just 6.6%. The rated power represents a ceiling value. In practice, varying BMS limits, thermal and electrical constraints, transport kinetics, and high SOC tapering of the battery would prevent a proportional reduction of time. This is consistent with findings in the XFC literature that within a rapid charging context, the acceptance of energy is predominantly a function of materials and the charging protocol, rather than the rating of the dispenser [2].H1 has been confirmed, but the significance of the nonlinearity is greater than that of the significance. The modeled average time of 13.9 minutes at 400 kW is an example of the goal of achieving 15-minute XFC, and is not a claim that all vehicles would achieve this. Significant cell-level (and pack-level) design and control would be required to achieve this, as evidenced by Wang et al. who were able to charge to a SOC of 75% within 12 minutes for over 900 cycles [3], and Tanim et al. who reported a 10-minute charge with at least 600 cycles and no lithium plating in the cells of their design [15]. Pack-level design and control is also required for the design of thermal control, the points at which the pack is electrically connected, and the way in which the electric current is distributed throughout the pack.

H2 and H3 both received support as increased power caused maximum temperatures and degradation stresses to rise. At high charge rates, the combination of the intercalated electrolyte and polarization can create a concentration gradient resulting in the deposition of lithium onto graphite. Inactive lithium wastes the previously usable lithium inventory [5,9–13]. In the case of a rapid charge, deposition occurs, and Extended Extreme Fast Charging (XFC) can cause the cathode to crack and the surface to reconstruct [13,14]. The relationship between temperature and deposition is complex. Controlled preheating can improve transport and help minimize deposition. However, high sustained temperatures can accelerate surface reactions and the growth of the Solid Electrolyte Interphase (SEI) [7,8,10]. In combination with the electrochemical design, post charge heat rejection is aggressive and thermally switching is applied [3,6,16].

Nickel rich NMC/NCA cells can pack a higher energy density at the cost of more careful design to manage the thermally and structurally active nature of the cell. LFP offers the opposite balance and can have a better cycle life. LTO is an improvement over LFP in that it can tolerate high charge and discharge rates, but it have a poor energy density [22]. Silicon in the anode can help with the electrode density, but adds the challenge of large volumetric changes. Solid state and lithium metal will push the fast charge limits, but do not have the fleet scale data to back the deployment. Without the pack and electrode design, SOC and temperature context, no chemistry can be given an arbitrary safe kW.

H4 was statistically supported; however, charging time was less variable compared to efficiency. The model's performance peak was around 250 kW, with a range of 150–400 kW showing values greater than 95%. A high voltage infrastructure will help, as I^2R losses will be reduced when power stays constant, as doubling the voltage will halve the current. SiC devices will operate in a high-voltage and high-frequency space; however, junction-temperature control will still be necessary [25]. The 400/800-V classification is a standard, but should not be taken too far, as real-world vehicles with their own unique configurations will not be able to support it. The classification only serves as a comparison of different architectures and does not support a variance in voltage.

The Impact of real-world deployment scales quickly, with 4 dispensers of 350 kW showing a 1.4 MW nameplate load (without auxiliary loads) and MCS moves charging into the multi-megawatt range [29]. NREL shows retail-site demand can peak and operate with increased demand of 250% and an annual increase of 88% in retail site energy costs [20]. Therefore, heavy-duty hubs will most likely require grid upgrades, smart charging, photovoltaics, and/or stationary storage [21]. In 96 XFC-plus-storage scenarios, Guittet et al. provide great examples of storage with a mean optimal charging cost of $0.59/kWh [22].

Higher-power standards do not remove operational limits. CCS power classes include examples around 350 kW [31]; ChaoJi aims for over 500 kW [30]; SAE J3400 formalizes the North American conductive interface [27,28]; and MCS introduces a megawatt pathway for heavy vehicles [29]. Reliability is equally important. A field trial in California reported 73.3% of the 655 public CCS ports tested were operational (according to the study's definition) [26]. An unavailable or derated 400 kW unit has less value in transport than a more reliable lower-power charger. The opportunity is therefore presented from a reliable and high average energy transfer combined with pre-conditioning, diagnostics, interoperability and grid-awareness and control.

Practical and Technological Implications:-

Automakers should publish reproducible SOC-window charging curves (instead of a single peak-kW figure). They should also consider pre-conditioning, the uniformity of cell temperature, detection of lithium plating and the adaptation of current as priority elements. Charger builders will benefit from high-voltage conversion, SiC devices, modular power blocks and actively cooled connectors. Those operating the networks should dimension sites against the capacity of transformers, tariffs, and utilization, employing stationary storage, PVs and managed charging to mitigate interconnection peaks. From a user's perspective, the kW rating of a dispenser is less important than the actual energy transfer during a practical 10-20 mins stop, and makes the model put in the 250-350 kW range a preferred engineering compromise for many high energy passenger EV situations. Beyond that range, increasingly significant thermal and grid impacts will overwhelm the benefits of faster charging.

Limitations and Future Research:-

This work provides a formalized framework, but still relies on controlled testing across multiple vehicles. Real-world vehicle classes have different pack sizes, varying electrode loadings, differing chemistries, aging states, ambient temperatures, and differing custom cooling and charging control strategies. The Degradation-Stress index is a screening variable, not a predictor for pack end-of-life, and the class-based 400/800-V assumption provides a coarse level of abstraction for existing systems. Future work should incorporate open access, time-resolved, and end-of-life data sets for thermal and aging across different chemistries. These may include the 10 min testing protocols on LFP, nickel-rich and silicon-rich cells, and the 10 min testing protocols for grid-connected charging hubs. Solid-state batteries, digital twins, and the other proposed technologies will require long-term testing and validation.

Conclusion:-

The feasibility of ultra-fast EV charging exists, but the charger rating is not the only factor determining the benefit. After reviewing 2,500 literature-constrained scenarios, the average time consumption between the 10th and 80th percentiles changed from 71.4 minutes at 50 kW charging to 13.9 minutes at 400 kW charging. With this scenario, the maximum modeled temperature and stress caused to the battery and system increased by 8° C and 2X, respectively. Charged system and battery efficiency increased as well, and peaked around 250 kW charging with around 95.6%, while the demand to the grid scaled by 5X. An important finding was that above 350 kW charging a significant increase in thermal and site-power requirements was found, while the benefit in time decreased and only 50 kW was saved, the average time saved was around 1 minute. Experimental evidence offers support that charging times which are less than 15 minutes are possible, however, there are real constraints in terms of the plating of lithium and degradation to the materials. High-voltage designs, high-performance SiC power converters, A/C control, BMS with improved modularity, robust and standardized connectors to the grid with managed services, and planning/provisioning of grid-side resources, should be designed with ultra-fast charging in mind.

References:-

1. Kale, N. B. (2026). A Review of Global Electric Vehicle Market Growth. Aethel Research Digest Juncture: An International Journal, 2(2), 1-18.
2. Dufek, E. J., Abraham, D. P., Bloom, I., Chen, B. R., Chinnam, P. R., Colclasure, A. M., ... & Weddle, P. J. (2022). Developing extreme fast charge battery protocols–A review spanning materials to systems. Journal of Power Sources, 526, 231129.
3. Wang, C. Y., Liu, T., Yang, X. G., Ge, S., Stanley, N. V., Rountree, E. S., ... & McCarthy, B. D. (2022). Fast charging of energy-dense lithium-ion batteries. Nature, 611(7936), 485-490.
4. Attia, P. M., Grover, A., Jin, N., Severson, K. A., Markov, T. M., Liao, Y. H., ... & Chueh, W. C. (2020). Closed-loop optimization of fast-charging protocols for batteries with machine learning. Nature, 578(7795), 397-402.
5. Colclasure, A. M., Tanim, T. R., Jansen, A. N., Trask, S. E., Dunlop, A. R., Polzin, B. J., ... & Smith, K. (2020). Electrode scale and electrolyte transport effects on extreme fast charging of lithium-ion cells. Electrochimica Acta, 337, 135854.
6. Liu, T., Yang, X. G., Ge, S., Leng, Y., & Wang, C. Y. (2021). Ultrafast charging of energy-dense lithium-ion batteries for urban air mobility. ETransportation, 7, 100103.
7. Liu, T., Ge, S., Yang, X. G., & Wang, C. Y. (2021). Effect of thermal environments on fast charging Li-ion batteries. Journal of Power Sources, 511, 230466.
8. Nair, S., Manickavasagam, K., & Rao, S. N. (2025). Machine learning for computation of droop controller coefficients to improve the frequency nadir and ROCOF of a stand-alone microgrid. International Journal of Information Technology, 17(1), 367-378.
9. Veerabhadra, J., & Nagaraja Rao, S. (2024). Comparative assessment of high gain boost converters for renewable energy sources and electrical vehicle applications. Energy Harvesting and Systems, 11(1), 20220144.
10. Reddy, M. R. P., Manjunatha, B. M., Reddy, P. Y., Rao, S. N., Agnihotri, A., Saravanan, T., ... & Rao, B. S. (2025, June). 3DOF-PID Controllers for Regulation of Voltage in Microgrid Pored by Hybrid Wind-PV-Battery-AE-FC. In 2025 International Conference on Computing Technologies (ICOCT) (pp. 1-7). IEEE.
11. Varanasi, P. K., Nagaraja Rao, S., & Duraiswamy, P. (2025). Intelligent control of double boost converter interfaced with multilevel inverter for electrical vehicle applications. Journal of The Institution of Engineers (India): Series B, 106(3), 939-947.
12. Konz, Z. M., McShane, E. J., & McCloskey, B. D. (2020). Detecting the onset of lithium plating and monitoring fast charging performance with voltage relaxation. ACS Energy Letters, 5(6), 1750-1757.
13. Ho, A. S., Parkinson, D. Y., Finegan, D. P., Trask, S. E., Jansen, A. N., Tong, W., & Balsara, N. P. (2021). 3D detection of lithiation and lithium plating in graphite anodes during fast charging. ACS nano, 15(6), 10480-10487.
14. Tanim, T. R., Yang, Z., Colclasure, A. M., Chinnam, P. R., Gasper, P., Lin, Y., ... & Jansen, A. N. (2021). Extended cycle life implications of fast charging for lithium-ion battery cathode. Energy storage materials, 41, 656-666.
15. Baragi, A. S., Machul, B. G., Krishnamurthy, M. D., Patil, R. A., Vadde, A., & Rao, S. N. (2024). Enhancing the wireless power transfer system performance and output voltage of electric scooters. Energy Harvesting and Systems, 11(1), 20230136.

16. Zeng, Y., Zhang, B., Fu, Y., Shen, F., Zheng, Q., Chalise, D., ... &Prasher, R. S. (2023). Extreme fast charging of commercial Li-ion batteries via combined thermal switching and self-heating approaches. Nature Communications, 14(1), 3229.
17. Das, R., Sachin, S., & Rao, S. N. (2026, February). Solar Powered Wireless Power Transfer System for Electric Vehicles Using a Push–Pull Converter with Intelligent MPPT Control. In 2026 International Conference on Computing, Electronics & Communications Engineering (ICCECE) (pp. 1-7). IEEE.
18. Huang, W., Ye, Y., Chen, H., Vilá, R. A., Xiang, A., Wang, H., ... & Cui, Y. (2022). Onboard early detection and mitigation of lithium plating in fast-charging batteries. Nature communications, 13(1), 7091.
19. Lee, S. M., Kim, J., Moon, J., Jung, K. N., Kim, J. H., Park, G. J., ... & Park, M. S. (2021). A cooperative biphasic MoO x–MoP x promoter enables a fast-charging lithium-ion battery. Nature communications, 12(1), 39.
20. Gilleran, M., Bonnema, E., Woods, J., Mishra, P., Doebber, I., Hunter, C., ... & Mann, M. (2021). Impact of electric vehicle charging on the power demand of retail buildings. Advances in Applied Energy, 4, 100062.
21. Zhu, X., Mishra, P., Mather, B., Zhang, M., & Meintz, A. (2023). Grid impact analysis and mitigation of en-route charging stations for heavy-duty electric vehicles. IEEE Open Access Journal of Power and Energy, 10, 141-150.
22. Guittet, D., Gasper, P., Shirk, M., Mitchell, M., Gilleran, M., Bonnema, E., ... & Mann, M. (2024). Levelized cost of charging of extreme fast charging with stationary LMO/LTO batteries. Journal of Energy Storage, 82, 110568.
23. Ahmad, A., Qin, Z., Wijekoon, T., & Bauer, P. (2022). An overview on medium voltage grid integration of ultra-fast charging stations: Current status and future trends. IEEE Open Journal of the Industrial Electronics Society, 3, 420-447.
24. Divyashree, B., Rao, S. N., & Veerabhadra. (2022). An Assessment of Criss-Cross Multilevel Inverter with Fault Tolerance for Electric Vehicle Applications. In Distributed Computing and Optimization Techniques: Select Proceedings of ICDCOT 2021 (pp. 153-163). Singapore: Springer Nature Singapore.
25. Shuai, Z., He, S., Xue, Y., Zheng, Y., Gai, J., Li, Y., ... & Li, J. (2023). Junction temperature estimation of a SiC MOSFET module for 800V high-voltage application in electric vehicles. Etransportation, 16, 100241.
26. Rempel, D., Cullen, C., Matteson Bryan, M., & Vianna Cezar, G. (2024). Reliability of open public electric vehicle direct current fast chargers. Human Factors, 66(11), 2528-2538.
27. Kozielski, K., Mudiyanselage, G. A., Narimani, M., & Emadi, A. (2025). A review of three-port integrated on-board charger and auxiliary power module in electric medium-and heavy-duty vehicles. IEEE Open Journal of Power Electronics, 6, 1347-1370.
28. Charging Interface Initiative. (2022). eV," Megawatt Charging System-Recommendations and requirements for MCS related standards bodies and solution suppliers,".